

# Quantification of Iron in Boron-Doped Silicon Solar Cells From Open Circuit Voltage Measurements

Axel Herguth , Member, IEEE

**Abstract**—Iron is one of the most commonly encountered contaminants in crystalline silicon. The peculiarity of interstitial iron to form iron-boron pairs under certain circumstances reveals its presence because of different electrical activity of interstitial and paired iron, and allows the quantification of the contamination level. In this article, it is shown by means of simulations how the iron contamination level in solar cells can be estimated from changes in open circuit voltage. It is further elaborated how measurements at different illumination intensities can be used to determine the contamination level more accurately. Furthermore, the impact of various error sources is analyzed.

**Index Terms**—Crystalline silicon, interstitial iron, iron-boron pairs, measurement technique, quantification, simulation, solar cells.

## I. INTRODUCTION

IRON is one of the most common contaminants in crystalline silicon, often being present in concentrations well above  $1 \times 10^{11} \text{ cm}^{-3}$  in unprocessed (non-gettered) wafers. However, thanks to the gettering effect of a phosphorous diffusion commonly used for emitter formation in p-type substrates, iron contamination is typically reduced by more than an order of magnitude [1], [2]. Nevertheless, iron is often still present above  $1 \times 10^{10} \text{ cm}^{-3}$  in processed, gettered solar cells, e.g., [3].

Unfortunately, interstitial iron is very recombination active and can strongly impair excess carrier lifetime, and in last consequence the performance of solar cells [4], [5]. This applies in particular to p-type material as it is exemplarily demonstrated in Fig. 1 by means of PC1D (mod 6.2) simulations for a state-of-the-art PERC structure (relevant simulation parameters in the caption). Above a contamination level of  $1 \times 10^{10} \text{ cm}^{-3}$  interstitial iron ( $\text{Fe}_i$ ) noticeably impacts the electrical performance, in particular, the short circuit current density  $j_{sc}$  and the fill factor  $FF$  but to a lesser extent also the open-circuit voltage  $V_{oc}$ . The stronger impact on  $j_{sc}$  than on  $V_{oc}$  is a specific signature of the strong asymmetric capture cross sections of interstitial iron for electrons and holes as discussed later on in more detail (see Table I and Fig. 2).

However, in p-type material, where the focus of this article lies, iron is present as interstitial species only in the presence

Manuscript received November 17, 2021; revised January 31, 2022, March 6, 2022, and April 9, 2022; accepted April 11, 2022. Date of publication May 2, 2022; date of current version June 21, 2022. This work was supported by the German Federal Ministry for Economic Affairs and Climate Action under Grant 03EE1051C.

The author is with the Department of Physics, University of Konstanz, 78457 Konstanz, Germany (e-mail: axel.herguth@uni-konstanz.de).

Color versions of one or more figures in this article are available at <https://doi.org/10.1109/JPHOTOV.2022.3168134>.

Digital Object Identifier 10.1109/JPHOTOV.2022.3168134

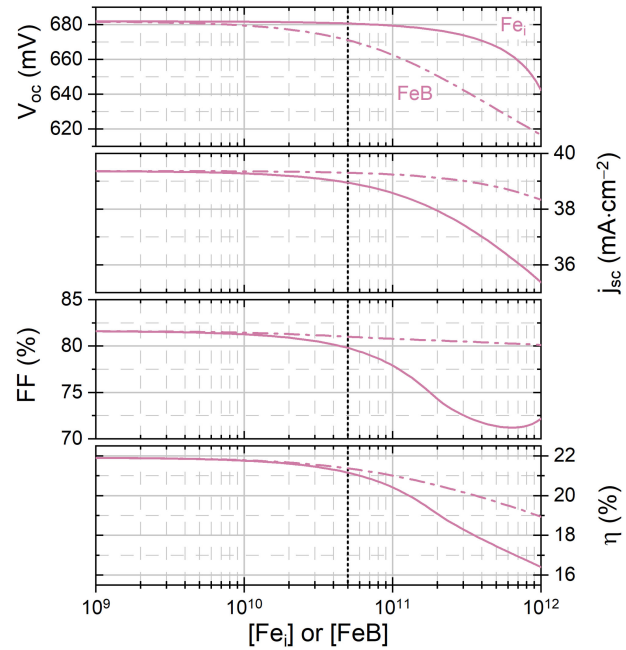


Fig. 1. Electrical parameters of a PERC-like solar cell impacted either by interstitial iron ( $\text{Fe}_i$ ) or iron-boron pairs ( $\text{FeB}$ ) obtained from a PC1D (mod 6.2) simulation. Cell parameters: Base doping  $1 \times 10^{16} \text{ cm}^{-3}$ , combined front and rear  $J_0 = 110 \text{ fAcm}^{-2}$ , otherwise intrinsic bulk lifetime limitation [9], thickness  $160 \mu\text{m}$ , lumped series resistance  $0.5 \Omega \text{ cm}^2$ . Temperature  $25^\circ\text{C}$ . Monochromatic illumination  $62 \text{ mWcm}^{-2}$  at  $800 \text{ nm}$  (generation-equivalent to 1 sun standard test conditions (STC) [10], [11]). No reflection losses. The vertical black dotted line marks the iron contamination level of  $5 \times 10^{10} \text{ cm}^{-3}$  used in Fig. 2.

TABLE I  
DEFECT-SPECIFIC PARAMETERS FROM LITERATURE [13], [16]

	$\sigma_n$ ( $\text{cm}^{-2}$ )	$\sigma_p$ ( $\text{cm}^{-2}$ )	$E_{\text{def}}$ (eV)
$\text{Fe}_i$	$4 \times 10^{-14}$	$7 \times 10^{-17}$	$E_v + 0.38$
$\text{FeB}$	$5 \times 10^{-15}$	$3 \times 10^{-15}$	$E_c - 0.26$

of sufficiently high free electron densities, i.e., in the presence of excess carriers generated for example by illumination [6], [7]. In darkness, with hardly any available free electrons, iron is predominantly positively charged and tends to bind to negatively charged dopant atoms like boron forming iron-boron pairs [6], [7]. In principle, the same applies to other acceptors like gallium ( $\text{FeGa}$  pairs) as well [8]. These iron-dopant complexes feature a strongly different recombination activity [7]. Boron-iron pairs, for example, exhibit almost symmetric capture cross sections (see Table I and Fig. 2). In consequence, the impact of  $\text{FeB}$  pairs

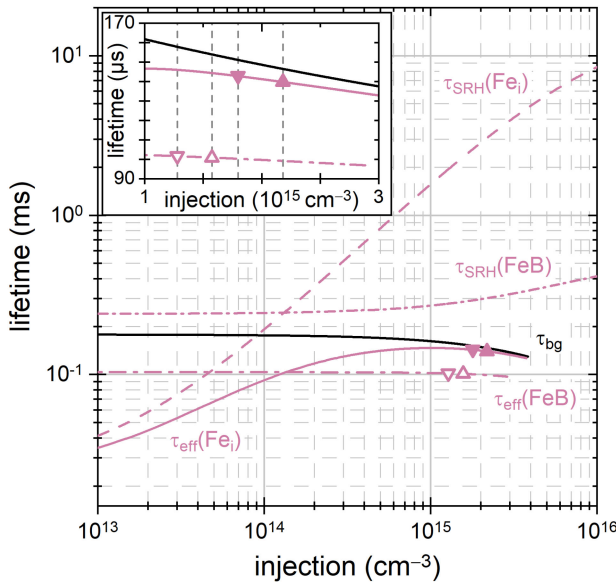


Fig. 2. Effective and  $\text{Fe}_i/\text{FeB}$ -related lifetime versus injection for an iron level of  $5 \times 10^{10} \text{ cm}^{-3}$ . PC1D simulation parameters correspond to those of Fig. 1. The black line shows the simulation not compromised by iron. The upward and downward triangles (and gray dashed lines in the inset) mark the respective injection in  $V_{\text{oc}}$  conditions obtained at  $62 \text{ mWcm}^{-2}$  or  $50 \text{ mWcm}^{-2}$  of monochromatic illumination at  $800 \text{ nm}$  without reflection losses. The inset is a close-up of the  $V_{\text{oc}}$  region in linear scaling.

on the performance of a solar cell is quite different as can be seen in Fig. 1 with a stronger impact on  $V_{\text{oc}}$  than on  $j_{\text{sc}}$ .

In fact, the different signature of recombination of the two iron species is a common way to qualitatively check for the presence of iron and to quantify (the switching part of) iron in crystalline silicon in lifetime samples with a sensitivity below  $1 \times 10^{10} \text{ cm}^{-3}$ , exceeding other elemental analysis techniques by far [7], [12], [13]. The procedure is quite simple. In the first step, a sample is kept in darkness for a sufficiently long duration to form the pairs. In the second step, excess carriers are injected (typically by high-intensity illumination) triggering the dissociation of the pairs. The comparison of injection-dependent lifetime measurements in the different states then allows for a quantification as explained in the later in more detail.

However, lifetime curves are not always available and tracking the observed change in electrical performance by device simulations can be a complex endeavor requiring many input parameters, and series resistance effects further complicate the analysis. Therefore, the question arises: What does the change in  $V_{\text{oc}}$  tell about the (switching part of) iron concentration?

Within this contribution, it is elaborated how a change in  $V_{\text{oc}}$  can be linked to a concentration of iron switching its state between  $\text{Fe}_i$  and  $\text{FeB}$ . Different approaches are presented and compared.

## II. BACKGROUND

### A. Impact of $\text{Fe}_i$ and $\text{FeB}$ on Lifetime

The impact of both defect species,  $\text{Fe}_i$  and  $\text{FeB}$ , on excess carrier lifetime can be described by Shockley, Read, and Hall's

theory of recombination at point defects [14], [15]. The corresponding lifetime component

$$\tau_{\text{SRH}} = \frac{\tau_n \cdot (p + p_1) + \tau_p \cdot (n + n_1)}{n \cdot p - n_i^2} = \frac{1}{f_{\text{def}} \cdot N_{\text{def}}} \quad (1)$$

depends on various quantities. On the one hand,  $\tau_{\text{SRH}}(\Delta n)$  crucially depends on excess carrier density (or injection)  $\Delta n$  defined as deviation of total electron and hole densities  $n = n_0 + \Delta n$  and  $p = p_0 + \Delta p$  from their respective equilibrium densities  $n_0$  and  $p_0$ . Neutrality typically implies  $\Delta n = \Delta p$ .

On the other hand, there are defect-specific properties such as electron and hole capture time constants  $\tau_{n,p} = (v_{n,p} \cdot \sigma_{n,p} \cdot N_{\text{def}})^{-1}$  comprising specific capture cross sections  $\sigma_{n,p}$  and the density of the defect species  $N_{\text{def}}$ .  $v_{n,p}$  denotes the respective thermal velocities. Note that the defect density can be factored-out, so that  $\tau_{\text{SRH}} \propto N_{\text{def}}^{-1}$  with the proportionality factor  $f_{\text{def}}(\Delta n)$  capturing the specific injection dependence. The quantities  $n_1$  and  $p_1$  relate to the statistical occupation of the defect-specific energy level  $E_{\text{def}}$  and thus depend on its position within the band gap. Commonly accepted values from the literature of the defect parameters are summarized in Table I.

Effective lifetime is a result of superposition of various recombination channels and may be written as

$$\frac{1}{\tau_{\text{eff}}} = \frac{1}{\tau_{\text{bg}}} + \frac{1}{\tau_{\text{SRH}}} = \frac{1}{\tau_{\text{bg}}} + f_{\text{def}} \cdot N_{\text{def}} \quad (2)$$

neglecting spatial effects because of inhomogeneous injection or alike. In the context of this article, it is deemed acceptable to summarize all recombination not related to  $\text{Fe}_i$  or  $\text{FeB}$  into a background lifetime  $\tau_{\text{bg}}$  of not exactly known injection dependence (even though it is precisely known here).

Fig. 2 demonstrates the impact of  $5 \times 10^{10} \text{ cm}^{-3}$   $\text{Fe}_i$  or  $\text{FeB}$  on the effective lifetime for the solar cell simulated in Fig. 1. As mentioned above,  $\text{FeB}$  features rather symmetric capture cross sections resulting in a rather flat injection dependence of the  $\text{FeB}$ -related lifetime component  $\tau_{\text{SRH}}(\text{FeB})$ . In contrast,  $\text{Fe}_i$  features strongly different capture cross sections for electrons and holes resulting in a strong injection dependence of the  $\text{Fe}_i$ -related lifetime component  $\tau_{\text{SRH}}(\text{Fe}_i)$ .

As can be seen, effective lifetime is higher for  $\text{Fe}_i$  than for  $\text{FeB}$  in the injection region above  $1 \times 10^{15} \text{ cm}^{-3}$ , where  $V_{\text{oc}}$  is typically found, resulting in  $V_{\text{oc}}(\text{Fe}_i) > V_{\text{oc}}(\text{FeB})$ . In fact, the  $\text{Fe}_i$ -related lifetime component is that high that it merely impacts  $\tau_{\text{eff}}$  here and there is hardly any loss in  $V_{\text{oc}}$  compared with simulation not compromised by iron (black line) that essentially corresponds to the background lifetime  $\tau_{\text{bg}}$ .

In the injection region around  $1 \times 10^{14} \text{ cm}^{-3}$  where the maximum power point is typically located,  $\tau_{\text{eff}}(\text{Fe}_i)$  shows a pronounced injection dependence (in contrast with  $\tau_{\text{eff}}(\text{FeB})$ ) implying a low fill factor  $FF$  (and high diode ideality factor) because effective lifetime is notably lower than at  $V_{\text{oc}}$ . Note the crossover point (cop) of  $\tau_{\text{eff}}(\text{Fe}_i)$  and  $\tau_{\text{eff}}(\text{FeB})$  in the low  $10^{14} \text{ cm}^{-3}$  range—a characteristic marker for iron contamination [12].

Toward even lower injection in the  $10^{13} \text{ cm}^{-3}$  range, conditions met under short-circuit conditions,  $\tau_{\text{eff}}(\text{Fe}_i)$  is stronger

limited compared with  $\tau_{\text{eff}}(\text{FeB})$ , implying stronger losses in short-circuit current (density)  $j_{\text{sc}}$ .

### B. Impact of Lifetime on $V_{\text{oc}}$

In steady-state illumination conditions, where mean recombination rate  $R$  balances mean generation rate  $G$ , effective lifetime  $\tau_{\text{eff}}$  can be deduced with knowledge of the excess carrier density (or injection)  $\Delta n$  being present according to

$$R = \frac{\Delta n}{\tau_{\text{eff}}} = G. \quad (3)$$

Note that (effective) lifetime typically depends on injection itself, and thus, determining the injection dependence of lifetime requires a variation of generation.

For a solar cell (with p-n junction) mass action law

$$n \cdot p = \Delta n^2 + \Delta n \cdot (n_0 + p_0) + n_0 p_0 = n_i^2 \cdot \exp\left(\frac{V_{\text{pn}}}{V_{\text{th}}}\right) \quad (4)$$

links p-n junction voltage  $V_{\text{pn}}$  and excess carrier density (or injection)  $\Delta n$  defined as deviation of total electron and hole densities  $n$  and  $p$  from their respective thermal equilibrium densities  $n_0$  and  $p_0$  in darkness. Mass action law further comprises mean thermal voltage  $V_{\text{th}} = k_B T / q$  given by Boltzmann's constant  $k_B$ , absolute temperature  $T$  and elementary charge  $q$ , as well as the (temperature-dependent) effective intrinsic carrier density  $n_i$ . Hence, effective lifetime  $\tau_{\text{eff}}$  can be deduced from known generation rate  $G$  and p-n junction voltage  $V_{\text{pn}}$ .

However, the actually measurable voltage  $V = V_{\text{pn}} + R_s \cdot I$  of a solar cell typically differs from p-n junction voltage  $V_{\text{pn}}$  because of a voltage drop  $\Delta V = R_s \cdot I$  across a series resistance  $R_s$  when a current  $I$  flows. Hence, p-n junction voltage  $V_{\text{pn}}$  can only be unambiguously extracted in open circuit conditions where no current is extracted and where open circuit voltage  $V_{\text{oc}}$  resembles p-n junction voltage  $V_{\text{pn}}$ . Hence, as discussed in [17] in great detail, a *Suns-V<sub>oc</sub>*-measurement [18], [19] rejecting series-resistance effects would be best suited for lifetime analysis as it offers information across a large injection range. However, that technique might not always be available, and the case where only  $V_{\text{oc}}$  values at certain illumination intensities are available shall be the focus of this article.

## III. IRON QUANTIFICATION FROM $V_{\text{oc}}$

Consider at first that  $V_{\text{oc}}$  is given *before* and *after* dissociation, i.e.,  $V_{\text{oc},B}$  dominated by FeB and  $V_{\text{oc},A}$  dominated by Fe<sub>i</sub>. The calculation of effective lifetimes  $\tau_{\text{eff},B}$  and  $\tau_{\text{eff},A}$  from (3), each valid at its specific injection  $\Delta n_B$  and  $\Delta n_A$ , is straightforward in this example because of the intentionally chosen monochromatic illumination at 800 nm (penetrating the emitter with negligible losses, but not reaching the rear side) and thus well known generation rate  $G$ . However, it should be noted that a different  $V_{\text{oc}}$  implies a different injection  $\Delta n$ , thus  $\Delta n_B \neq \Delta n_A$  if  $V_{\text{oc},B} \neq V_{\text{oc},A}$ .

Following (2) and assuming that the dissociation is complete, i.e.,  $[\text{FeB}]_B = [\text{Fe}_i]_A = [\text{Fe}]$  with  $[\text{Fe}]$  being the true iron contamination capable of switching states (not bound in clusters),

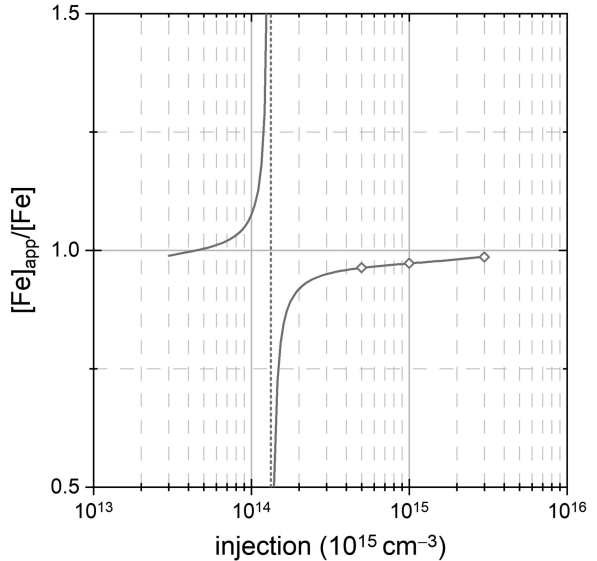


Fig. 3. Ratio of apparent and true iron contamination derived from the *Suns-V<sub>oc</sub>* approach at different injection  $\Delta n$  for the scenario shown in Fig. 2 with an iron contamination  $[\text{Fe}] = 5 \times 10^{10} \text{ cm}^{-3}$ . The symbols mark the injection levels depicted in Fig. 4.

these effective lifetimes yield a set of equations

$$\frac{1}{\tau_{\text{eff},A}} = \frac{1}{\tau_{\text{bg},A}} + f_{\text{Fe},A} \cdot [\text{Fe}] \quad (5)$$

$$\frac{1}{\tau_{\text{eff},B}} = \frac{1}{\tau_{\text{bg},B}} + f_{\text{FeB},B} \cdot [\text{Fe}]. \quad (6)$$

If either a certain fraction of FeB pairs remains or Fe<sub>i</sub> already exists, their impact on lifetime contributes to  $\tau_{\text{bg}}$  and cannot be quantified. See Section IV-C for information on the completeness of dissociation. In this respect,  $[\text{Fe}]$  rather refers only to the fraction of iron switching its state. These equations may be exploited in different ways as discussed in the following.

### A. Suns- $V_{\text{oc}}$ Approach

As *Suns-V<sub>oc</sub>* measurements determine  $V_{\text{oc}}$  at various generation rates, and thus offer information in a broad range of injection levels, it should be possible to extract  $\tau_{\text{eff},B}(\Delta n)$  and  $\tau_{\text{eff},A}(\Delta n)$  at a common injection level  $\Delta n$ . In this case, the contribution of the non-iron related background lifetime is the same, i.e.,  $\tau_{\text{bg},B}(\Delta n) = \tau_{\text{bg},A}(\Delta n)$ , and cancels out. Iron contamination then follows from (5) and (6):

$$[\text{Fe}]_{\text{app}} = \frac{\frac{1}{\tau_{\text{eff},A}} - \frac{1}{\tau_{\text{eff},B}}}{f_{\text{Fe},A} - f_{\text{FeB},B}}. \quad (7)$$

This corresponds to the classical approach for iron quantification from injection-dependent lifetime data [12], [13] and yields an apparent iron contamination  $[\text{Fe}]_{\text{app}}(\Delta n)$  across a broad range of injection  $\Delta n$ . This is exemplarily shown in Fig. 3 for the scenario depicted in Fig. 2 with a true iron contamination of  $[\text{Fe}] = 5 \times 10^{10} \text{ cm}^{-3}$ . As can be seen,  $[\text{Fe}]_{\text{app}}$  deviates from  $[\text{Fe}]$  in a very characteristic way with an asymmetric pole as a result of the division by small numbers or differences as  $\Delta n$

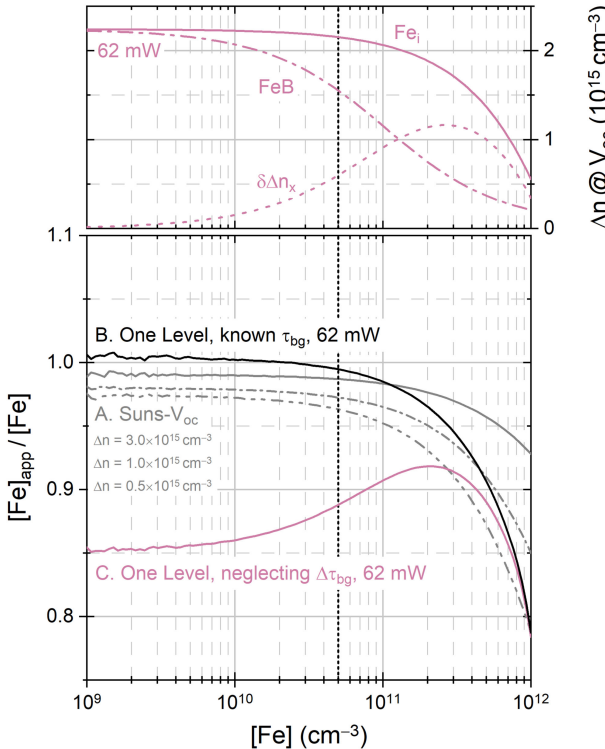


Fig. 4. (Top) Injection  $\Delta n$  obtained in  $V_{oc}$  conditions and the injection mismatch  $\delta\Delta n$ . (Bottom) Ratio of apparent and true iron contamination derived from A.) the *Suns- $V_{oc}$*  approach evaluated at different injection  $\Delta n$ , B.) the one intensity level approach with known background lifetime, C.) the one intensity level approach neglecting the change in background lifetime  $\tau_{bg}$ . The vertical black dotted line marks the iron contamination level of  $5 \times 10^{10} \text{ cm}^{-3}$  used in Fig. 2.

approaches the crossover point at  $1.3 \times 10^{14} \text{ cm}^{-3}$ , implying  $\tau_{eff,B} \rightarrow \tau_{eff,A}$  and  $f_{Fe,A} \rightarrow f_{FeB,B}$ . In general, the assessment of iron contamination becomes more reliable the further away the injection level from the crossover point is.

The gray lines in Fig. 4 show the performance of the *Suns- $V_{oc}$*  approach at selected injection levels with varying iron contamination. As can be seen, the *Suns- $V_{oc}$*  approach fairly approximates the true iron contamination, the better the higher the injection level  $\Delta n$  chosen for evaluation. However, it should be noted that the required intensity/generation to reach a certain injection level unavoidably increases with dropping lifetime. Therefore, high injection levels are generally harder to obtain for high iron contamination and might not be obtainable in experiment. For example, lifetime drops to  $\sim 10 \mu\text{s}$  for  $[Fe] = 1 \times 10^{12} \text{ cm}^{-3}$  and requires more than a tenfold higher intensity to obtain a certain injection level than the scenario shown in Fig. 2. It is therefore likely that the analysis has to be carried out at lower injection levels for higher iron levels, and in consequence, iron contamination is likely stronger underestimated.

Furthermore, contamination tends to be underestimated at very high iron levels because lifetime and thus diffusion length drops, and with that the assumption of a homogeneous injection in depth is increasingly compromised. In numbers, FeB-related lifetime drops to  $\sim 10 \mu\text{s}$  for  $[Fe] = 1 \times 10^{12} \text{ cm}^{-3}$ . That corresponds to a diffusion length similar to cell thickness. In consequence, injection varies from front to rear of the cell and the

injection derived from p-n junction voltage (at the front) is not a reliable measure of average injection. However, iron contamination exceeding  $1 \times 10^{11} \text{ cm}^{-3}$  is rarely found in gettered solar cells, and thus, the issue of inhomogeneous injection is rather irrelevant in reality.

### B. One Intensity Level Approach with Known Background

But the focus of this article shall lie on the scenario where  $V_{oc}$  is known only at one intensity level (or later at two) *before* and *after* FeB dissociation, likely from the measurement of the current-voltage characteristic at 1 sun intensity (photon-flux equivalent to  $62 \text{ mWcm}^{-2}$  monochromatic illumination at 800 nm [11]). Note that  $V_{oc,B} \neq V_{oc,A}$  implies  $\Delta n_B \neq \Delta n_A$ , and thus, the analysis cannot be done at a common injection. Apparent iron contamination follows from (5) and (6):

$$[Fe]_{app} = \frac{\left(\frac{1}{\tau_{eff,A}} - \frac{1}{\tau_{eff,B}}\right) - \left(\frac{1}{\tau_{bg,A}} - \frac{1}{\tau_{bg,B}}\right)}{f_{Fe,A} - f_{FeB,B}} \quad (8)$$

but this time, background lifetime is sampled at different injection levels, i.e.,  $\tau_{bg,B}(\Delta n_B) \neq \tau_{bg,A}(\Delta n_A)$ , and therefore, does not cancel out.

The advantage of the simulation here is that background lifetime is known from the reference scenario not compromised by iron (black line in Fig. 2). Hence, iron contamination can be calculated from (8) in order to check whether the set of equations describes the situation correctly or not. This is evaluated with the  $V_{oc}$  data from Fig. 1. As can be seen from Fig. 4, the ratio of apparent iron contamination  $[Fe]_{app}$  and true iron contamination  $[Fe]$  is close to unity up to  $[Fe] \sim 1 \times 10^{11} \text{ cm}^{-3}$  if the change in background lifetime is taken into account (black line). Above that, the deviation between apparent and true iron contamination increases stronger than in the *Suns- $V_{oc}$*  approach. Apart from the issue of inhomogeneous injection with depth, the analysis of  $V_{oc}$  data obtained from fixed intensity/generation implies that analysis takes place at decreasing injection levels for increasing iron contamination because of the drop in overall lifetime (Fig. 4 top). Hence, the analysis does not follow one of the gray curves in Fig. 4, but rather switches gradually from the higher injection curve to the low injection curve with increasing iron contamination, and in consequence, the black curve drops stronger than each of the gray curves does.

Nevertheless, the idealized analysis with just  $V_{oc}$  data obtained at 1 sun fixed intensity works fine in the contamination range below  $1 \times 10^{11} \text{ cm}^{-3}$ .

### C. One Intensity Level Approach with Unknown Background

However, in reality background lifetime is unknown, and thus, the set of equations (5) and (6) comprise three unknown quantities: the iron contamination level  $[Fe]$  intended to be quantified and the background lifetime  $\tau_{bg}$  evaluated at different injections. All other quantities are known. From a mathematical point of view, this is an underdetermined system without a unique solution.

The most simple approach to solve this problem is to assume that the background lifetime does not vary with injection, i.e.,  $\tau_{bg,B}^* = \tau_{bg,A}^*$ , even though this is not necessarily true looking

at the inset of Fig. 2 (black line). Nevertheless, this assumption eliminates one unknown quantity and thus the whole second bracket in (8), and allows for a unique solution.

This simple approach is evaluated with the  $V_{oc}$  data from Fig. 1 using an intensity of  $62 \text{ mWcm}^{-2}$ . The results are depicted in Fig. 4 (red line). As can be seen, the ratio of apparent and true iron contamination  $[\text{Fe}]_{\text{app}}/[\text{Fe}]$  is fairly close to unity with a slight underestimation by 10%–15% and light dependence on  $[\text{Fe}]$ . A comparison of the injection range obtained under  $V_{oc}$  conditions with Fig. 2 reveals that injection is (except for the very high  $[\text{Fe}]$  values) in a range where background lifetime notably changes with injection, and the injection mismatch  $\delta\Delta n = \Delta n_A - \Delta n_B$  between the measurements suggests that this dependency correlates with the injection mismatch.

Repeating the same analysis with lower intensities down to  $10 \text{ mWcm}^{-2}$  (1/6 sun) is quite instructive. As shown in the bottom part of Fig. 5, the gap between apparent and true iron contamination closes when a lower intensity is used. This improvement indicates that the change in background lifetime becomes less relevant toward lower intensity. This is consistent with Fig. 2 where background lifetime saturates toward lower injection. Hence, one might argue that using even lower intensities might be advantageous for a more accurate quantification of iron. However, there occurs an asymmetric pole that moves toward lower iron contamination with lower intensity. For ease of reading, data above the poles are not shown here. These poles occur when  $V_{oc}(\text{FeB})$  and  $V_{oc}(\text{Fe}_i)$  curves cross (see Fig. 5 top) indicating that the crossover point (cop) in injection  $\Delta n_{\text{cop}}$  at  $1.3 \times 10^{14} \text{ cm}^{-3}$  is reached (see Fig. 5 middle). However, a slight increase in  $V_{oc}(\Delta n_{\text{cop}})$  and  $\Delta n_{\text{cop}}$  is visible toward highest iron levels as a result of increasing inhomogeneity of injection in depth. In retrospect, the stronger drop of the red 62 mW curve in Fig. 4 is related to the drop toward a pole lying above  $[\text{Fe}] = 1 \times 10^{12} \text{ cm}^{-3}$ , and thus, outside the depicted range.

In summary,  $V_{oc}$  analysis at fixed intensity generally suffers from a similar problem as the *Suns-V<sub>oc</sub>* analysis (see Fig. 3), and the ideal intensity would be in a range high enough to avoid the pole problematic and where the change in background lifetime is rather weak. For the state-of-the-art PERC cell simulated here with a rather flat injection dependence toward low injection, the best range to determine iron contamination typically lying in the low  $1 \times 10^{10} \text{ cm}^{-3}$  range would be  $\sim 1/6$  sun. However, in the case of a strong injection dependence of background lifetime, Fig. 5 might look different and reducing intensity might not always be advisable. Nevertheless, even a deviation of 10 to 15% at 1 sun intensity is not bad in view of the simplicity of the approach, in particular, if  $V_{oc}$  data at 1 sun are known from standard cell analysis anyway.

#### D. Two Intensity Level Approach

The general problem of the one intensity level approach is that the set of equations (5) and (6) is underdetermined or, in other words, there is a lack of available information. Sometimes, solar cells are measured not only at one specific intensity (likely 1 sun, STC [10]) but at different intensity levels. The advantage is that the performance under different illumination conditions can be better assessed as solar cells often behave nonlinearly mainly

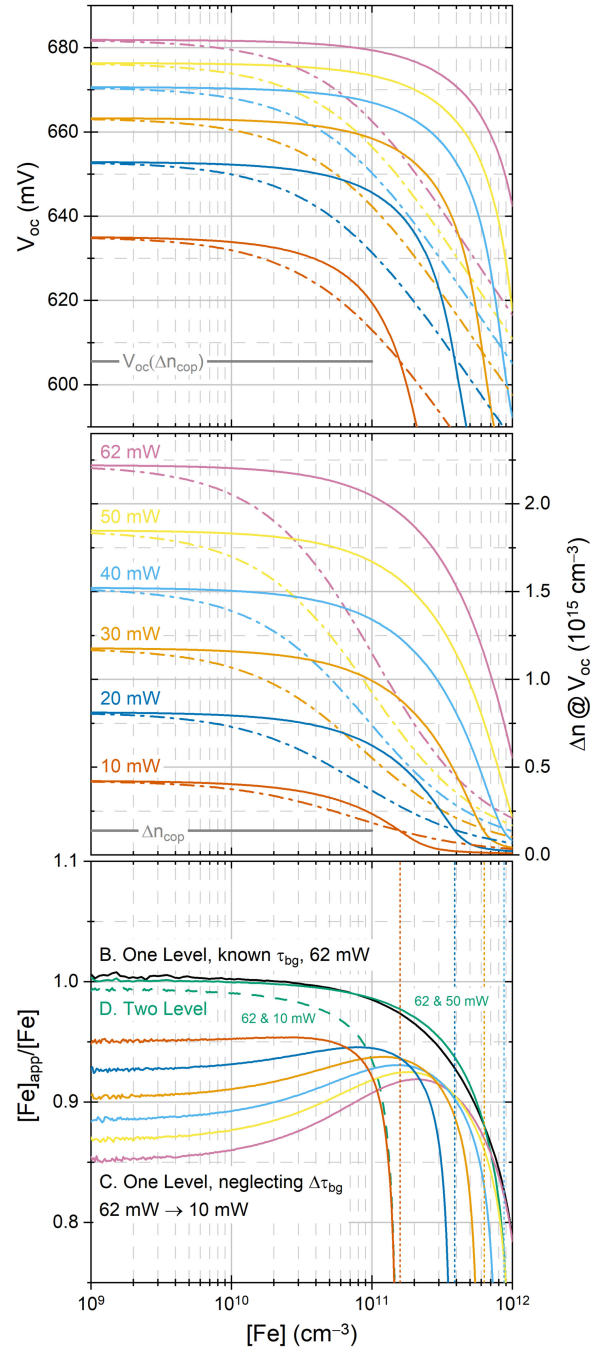


Fig. 5. Iron quantification with the one intensity level approach evaluated at different intensities. (Top)  $V_{oc}$  versus true iron contamination  $[\text{Fe}]$  with iron being either in the paired FeB state (dashed lines) or in interstitial state  $\text{Fe}_i$  (continuous lines). (Middle) Derived injection present at  $V_{oc}$ . (Bottom) Apparent versus true iron contamination for the analysis with the one intensity level (B+C) approach at different intensities. The green lines relate to the analysis with the two intensity level approach (D). Data above the poles (marked by vertical pointed lines) are not shown to improve readability.

because of a changing impact of series resistance on fill factor and efficiency with changing intensity (current extraction). In this case, there is more information available that can be used to evaluate the iron contamination.

Therefore, consider in the following the situation where two measurements *before* (mainly FeB) and *after* dissociation (mainly  $\text{Fe}_i$ ) at two different intensities, e.g.,  $62 \text{ mWcm}^{-2}$

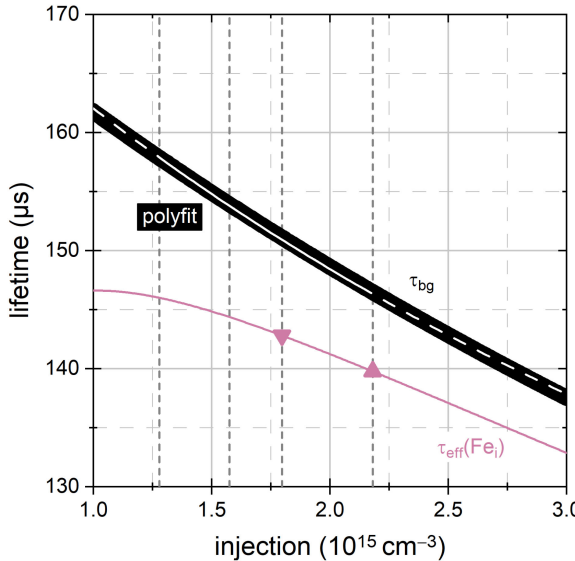


Fig. 6. Close-up of the lifetime range from Fig. 2 where the analysis with the two intensity level approach with 62 and 50 mWcm<sup>-2</sup> is performed. The white line shows the estimated background lifetime (continuous: interpolation, dashed: extrapolation), whereas the thick black line represents the background lifetime from the simulation not compromised by iron. The gray lines mark the injection levels present in  $V_{oc}$  conditions in the  $Fe_i$  (A1, A2) and FeB state (B1, B2) at high and low illumination intensity (upward and downward triangle).

( $\approx 1.0$  sun) and 50 mWcm<sup>-2</sup> ( $\approx 0.8$  sun) monochromatic at 800 nm, are available, named conditions (A1, A2) and (B1, B2) in the following. Most probably, obtained injection under  $V_{oc}$  conditions will not coincide as exemplarily depicted in Fig. 2, and thus, background lifetime is now probed at four injection levels. Hence, one can try to estimate the change in background lifetime  $\tau_{bg}(\Delta n)$  with injection by approximating its inverse by a polynomial (Taylor series)

$$\frac{1}{\tau_{bg,x}} = \alpha + \beta \cdot \delta n_x + \gamma \cdot \delta n_x^2 \quad (9)$$

with  $\alpha$  corresponding to the value of  $1/\tau_{bg}$  at a reference injection  $\Delta n_{ref}$ ,  $\beta$  to slope (first derivative),  $\gamma$  to curvature (second derivative), and  $\delta n_x = \Delta n_x - \Delta n_{ref}$  to the deviation of injection  $\Delta n_x$  present in condition  $x$  from the reference injection. The set of equations (5) and (6) has to be rewritten accordingly including the polynomial approach (9) for  $\tau_{bg}$ , yielding four equations describing the conditions  $x = (A1, A2, B1, B2)$ , and four unknown parameters ( $\alpha, \beta, \gamma$  and [Fe])

$$\frac{1}{\tau_{eff,x}} = \alpha + \delta n_x \cdot \beta + \delta n_x^2 \cdot \gamma + f_x \cdot [Fe]. \quad (10)$$

This linear equation system now has a unique solution. Fig. 6 shows the situation from the inset of Fig. 2 together with the polynomial fit for the background lifetime (9) demonstrating that change in background lifetime is well approximated. Fig. 5 (bottom) shows that the determined iron contamination level is almost perfectly similar to the approach with known background lifetime (black line) using 62 and 50 mWcm<sup>-2</sup> intensity (continuous green line). Only for very high iron contamination levels, the two intensity level approach increasingly fails. Repeating the analysis with a lower intensity of 10 instead of 50 mWcm<sup>-2</sup>

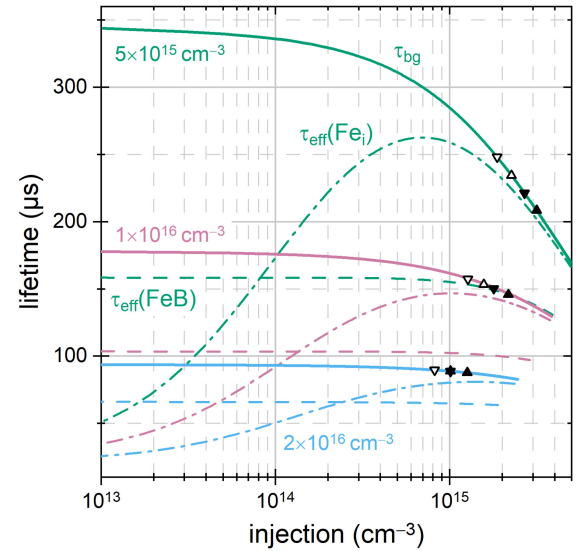


Fig. 7. Effective lifetime in the iron-free ( $\tau_{bg}$ ) as well as in the  $Fe_i$  and FeB state versus injection for an iron level of  $5 \times 10^{10}$  cm<sup>-3</sup>. PC1D simulation parameters correspond to those of Fig. 1 except for a variation in base doping ( $5 \times 10^{15}$ ,  $1 \times 10^{16}$ , and  $2 \times 10^{16}$  cm<sup>-3</sup>). The upward and downward triangles mark the background lifetime at the respective injection in  $V_{oc}$  conditions obtained at 62 or 50 mWcm<sup>-2</sup> of monochromatic illumination at 800 nm without reflection losses.

(dashed green line) shows that the curve drops toward the pole of the lower intensity measurement. Hence, using two rather high intensity measurements seems beneficial.

In conclusion, the two intensity level approach has the potential to outperform the one level approach because it estimates and eliminates the change in background lifetime being the driver behind the underestimation of iron contamination in the one level approach.

#### E. Impact of Base Doping

The exact injection dependence of the individual lifetime components and that of the resulting effective lifetime depends on the base doping of the solar cell. That holds true for bulk recombination described by the SRH-formalism (1) as well as for surface/emitter related lifetime  $\tau_{surf}$  described by the  $J_0$  formalism

$$\frac{1}{\tau_{surf}} = \frac{p_0 + \Delta n}{q w n_i^2} \cdot J_0 \approx \frac{1}{\tau_{bg}} \quad (11)$$

where  $q$  denotes the elementary charge,  $w$  the thickness of the cell, and  $J_0$  is a measure of surface recombination independent from injection and base doping [20], [21]. In the scenario of highly efficient solar cells described here (iron-free) background lifetime  $\tau_{bg}$  is essentially determined by surface recombination. As an example, the effective lifetimes for the scenario depicted in Fig. 2 are shown in Fig. 7 but this time with variable base doping  $p_0$  of  $5 \times 10^{15}$ ,  $1 \times 10^{16}$ , and  $2 \times 10^{16}$  cm<sup>-3</sup>. Note that the chosen factor of two corresponds to the typical doping variation in a boron-doped crystal. Two features can be seen from (11) and Fig. 7. First, toward low injection ( $\Delta n \ll p_0$ )  $\tau_{bg} \propto p_0^{-1}$  is flat and drops with higher doping  $p_0$ . Second, toward higher injection ( $\Delta n \gg p_0$ )  $\tau_{bg} \propto \Delta n^{-1}$  drops with injection

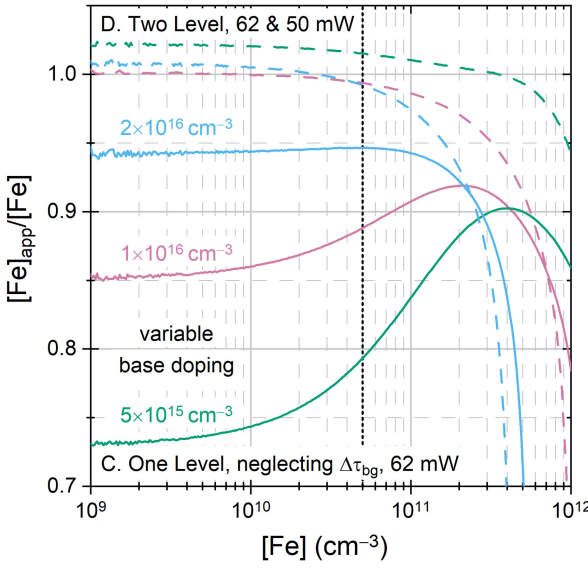


Fig. 8. Ratio of apparent and true iron contamination derived either from the one intensity level approach neglecting the change in background lifetime  $\tau_{bg}$  (C. using  $62 \text{ mWcm}^{-2}$ ) or the two intensity level approach (D. using 62 and  $50 \text{ mWcm}^{-2}$ ) with variable base doping. The vertical black dotted line marks the iron contamination level of  $5 \times 10^{10} \text{ cm}^{-3}$  used in Fig. 7.

$\Delta n$ . Obtained injection at  $V_{oc}$  (marked in Fig. 7 for the  $\text{Fe}_i$  and  $\text{FeB}$  state for an intensity of 50 and  $62 \text{ mWcm}^{-2}$ ) lies in the transition region where  $\Delta n \approx p_0$ . For a low base doping of  $5 \times 10^{15} \text{ cm}^{-3}$  (green line),  $\tau_{bg}$  starts on a high level and already exhibits a strong drop with injection in the  $V_{oc}$  region. In contrast, for a high base doping of  $2 \times 10^{16} \text{ cm}^{-3}$  (blue line),  $\tau_{bg}$  starts on a low level and shows hardly any decrease with injection in the  $V_{oc}$  region (being shifted toward lower injection for lower effective lifetimes because  $\Delta n = \tau_{eff} \cdot G$ ).

As discussed before, significant injection-dependent changes in background lifetime between the  $\text{Fe}_i$  and  $\text{FeB}$  state are a source of error in the one intensity level approach, and repeating the one intensity level analysis from Fig. 4 with variable base doping (see Fig. 8) confirms that iron contamination is underestimated to a greater extent in lowly doped material with the one intensity level approach even though reducing the intensity as discussed before might help to some extent.

Obviously, even the fact that the crossover point  $\Delta n_{cop}$ , at which  $\tau_{eff}(\text{Fe}_i) = \tau_{eff}(\text{FeB})$ , shifts to lower injection for lower doped material, while injection  $\Delta n(V_{oc})$  obtained at  $V_{oc}$  increases at the same time because of a generally increased effective lifetime, thus increasing the distance between  $\Delta n(V_{oc})$  and  $\Delta n_{cop}$ , does not improve iron quantification via the one intensity level approach even though it would be expected in a  $Suns-V_{oc}$  analysis (see Fig. 3). On the contrary, the generally lower lifetime for higher doped material in combination with a  $\Delta n_{cop}$  shifting toward higher injection implies that a lower iron contamination is sufficient to match  $\Delta n_{cop}$  and  $\Delta n(V_{oc})$  where  $\tau_{eff}(\text{Fe}_i) = \tau_{eff}(\text{FeB})$  resulting in the drop of the blue data toward a pole even within the studied iron contamination range in Fig. 8.

In direct comparison, the two intensity level approach (anticipating the change in background lifetime) yields superior results virtually independent of the doping level where it is

unclear whether the deviation from unity might be a result of inconsistently used intrinsic carrier density  $n_i$  (models) here [22] and in PC1D [23]. Note that the dashed lines of the two intensity level approach in Fig. 8 drop toward the  $50 \text{ mWcm}^{-2}$  poles, while the continuous lines of the one intensity level approach drop toward the  $62 \text{ mWcm}^{-2}$  poles.

#### IV. ERROR ESTIMATION

The presented method for iron contamination level quantification relies on four quantities: Generation rate  $G$ , temperature  $T$ , doping level  $p_0$  and open-circuit voltage  $V_{oc}$ . Each might be erroneous to a certain degree. However, errors in  $V_{oc}$  are often caused by unrecognized errors in temperature and generation. As derived in the Appendix,  $V_{oc}$  is known to depend strongly on temperature with a temperature coefficient

$$\frac{\partial V_{oc}}{\partial T} \approx \frac{1}{T} \cdot \left( V_{oc} - \frac{E_g}{q} \right) \quad (12)$$

being in the range of  $-1.5$  to  $-2.0 \text{ mV per } ^\circ\text{C}$  at  $25^\circ\text{C}$  depending on the actual  $V_{oc}$  level.

On the other hand,  $V_{oc}$  depends on generation  $G$ . As derived in the Appendix, the one diode model estimates the change in  $V_{oc}$  with normalized generation  $g = G/G_0$

$$\frac{\partial V_{oc}}{\partial g} \cdot \delta g = \frac{kT}{q} \cdot \delta g \quad (13)$$

to lie in the range of  $0.25 \text{ mV per \% generation fluctuation } \delta g = \delta G/G_0$  at  $25^\circ\text{C}$ .

Therefore, errors in  $V_{oc}$  are not treated separately in the following but rather considered as a part of errors in temperature and generation.

There are two types of errors that have to be taken into account: systematic errors that affect measurements in all conditions (*after* and *before*  $\text{FeB}$  dissociation) in the same way and fluctuation errors that affect the measurement in each condition independently. The effect is different as discussed in the following.

##### A. Systematic Errors

To investigate the impact of systematic errors on the resulting apparent iron contamination  $[\text{Fe}]_{app}$ , the existing simulations done at fixed temperature  $T$ , generation  $G$  and doping level  $p_0$  were retained, but the evaluation procedure was performed with deviating values  $T \pm 1^\circ\text{C}$ ,  $G \pm 5\%$  and  $p_0 \pm 10\%$ . The results are shown in Fig. 9.

As can be seen, systematic errors in all aforementioned quantities cause a constant factor of the apparent iron contamination  $[\text{Fe}]_{app}$  (constant shift in the ratio to the true contamination  $[\text{Fe}]$ ) irrespective of the contamination level. This holds true for both presented methods with one or two intensity levels. The relative error in  $[\text{Fe}]_{app}$  is of the order of  $6\%$  per  $K$  temperature error,  $1\%$  per  $\%$  relative generation error and  $0.4\%$  per  $\%$  relative doping level error. The reaction to positive and negative input variations is slightly different pointing to a nonlinear error response. Of course, systematic errors should be avoided if somehow possible but the error potential in the single-digit percentage range is rather limited.

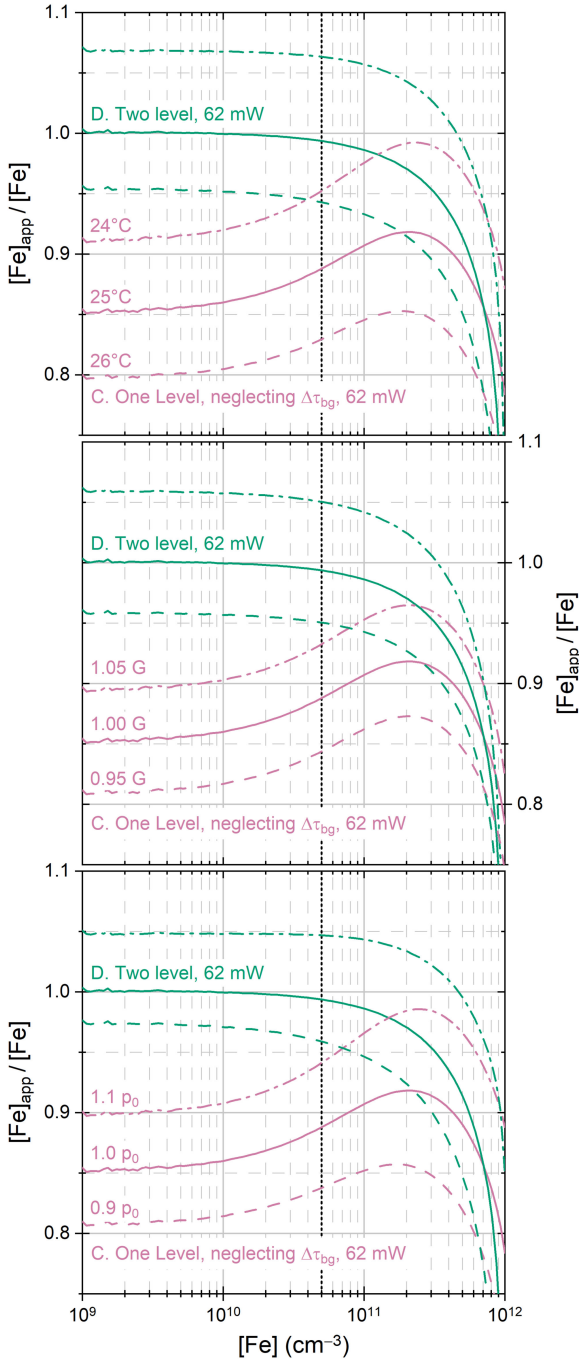


Fig. 9. Changes in apparent iron contamination level  $[Fe]_{app}$  because of systematic errors of  $\pm 1^\circ\text{C}$  in temperature (top),  $\pm 5\%$  in generation (middle) and  $\pm 10\%$  in doping level (bottom) based on the reference scenario shown in Fig. 4. The vertical black dotted line marks the iron contamination level of  $5 \times 10^{10} \text{ cm}^{-3}$  used in Fig. 2.

### B. Fluctuation Errors

The more relevant error source for application are probably unrecognized fluctuations, in particular of temperature and generation, between the measurements. This can be either because of the lack of precision in data storage or measurement inaccuracy/noise. As mentioned before,  $V_{oc}$  is strongly temperature-dependent. Hence, even though  $V_{oc,A}(\text{Fe}_i)$  should be higher than  $V_{oc,B}(\text{FeB})$ , one can easily construct a scenario where the

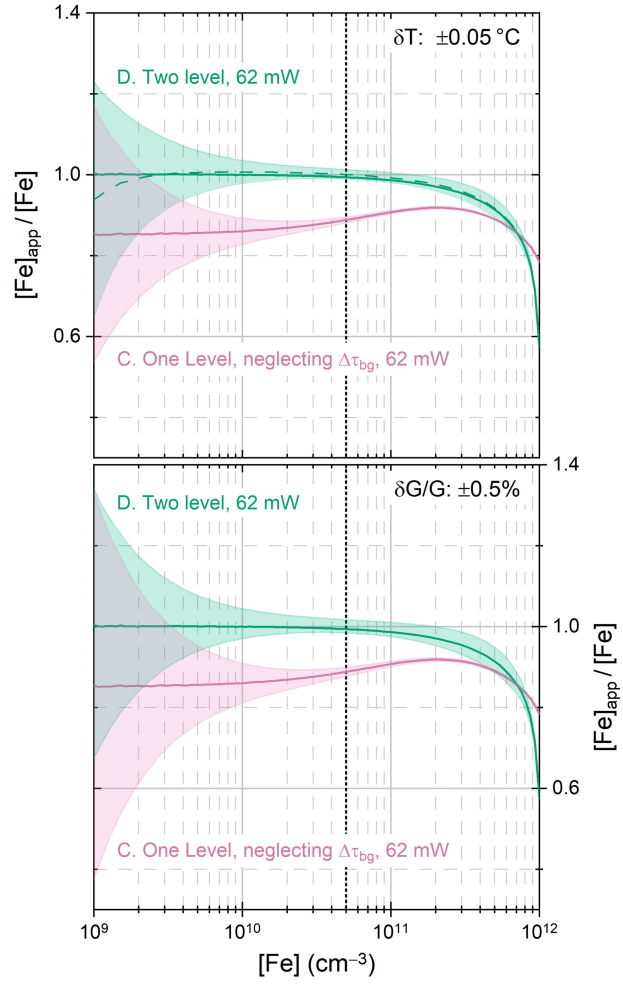


Fig. 10. Scattering in apparent iron contamination  $[Fe]_{app}$  as a result of unrecognized temperature (top) and generation fluctuations (bottom) between the measurements *before* and *after* FeB dissociation. The shaded area marks the results within one standard deviation from the reference scenario shown in Fig. 4 (solid lines). For the two level approach, there is a slight trend to underestimation as the mean value (dashed line) deviates from the reference scenario toward low contamination levels. The vertical black dotted line marks the iron contamination level of  $5 \times 10^{10} \text{ cm}^{-3}$  used in Fig. 2.

measurement temperature is unintentionally higher in the  $\text{Fe}_i$  state than in the  $\text{FeB}$  state and the iron contamination is that low that the temperature mismatch completely negates the  $V_{oc}$  difference caused by FeB dissociation.

In order to study the effect of unrecognized temperature fluctuations, the PC1D simulations done at  $25^\circ\text{C}$  were again retained, but temperatures *after* and *before* FeB dissociation used for calculation of  $[Fe]_{app}$  were randomized assuming uniformly distributed temperature fluctuations  $\delta T = \pm 0.05^\circ\text{C}$  (e.g., as a result of data being stored only with the first decimal place). The resulting normal-like distribution of  $[Fe]_{app}$  was quantified in terms of its standard deviation. The shaded areas shown in the upper part of Fig. 10 depict this range. As expected, low iron contamination levels are affected the most because the voltage difference is rather small there. The two intensity level approach shows comparable deviations as the one level approach with a slight trend to underestimation toward low contamination levels (dashed line deviating from the error-free solid green line

from Fig. 5) and nonvanishing small deviation toward higher contamination levels. However, one should note that the standard deviation only covers 68% of results and there are already some temperature combinations where the calculation fails for the lowest iron contamination level and results in negative values. From the voltage difference of 0.25 mV at a iron contamination level of  $1 \times 10^9 \text{ cm}^{-3}$  and a temperature coefficient of approximately  $-1.5 \text{ mV per } ^\circ\text{C}$  one can deduce that a temperature difference of  $0.16^\circ\text{C}$  (thus,  $\pm 0.08^\circ\text{C}$ ) leads to the described scenario where unfortunate temperature fluctuation completely negates the effect of FeB dissociation. Or in other words, only for unrecognized temperature fluctuations below  $\pm 0.08^\circ\text{C}$ , an iron contamination level of  $1 \times 10^9 \text{ cm}^{-3}$  can be reliably detected.

Hence, one can conclude that even though quantifying iron contamination in the low  $1 \times 10^9 \text{ cm}^{-3}$  range should be possible it certainly requires a high level of temperature control and measurement quality.

The same approach for error assessment was chosen for unrecognized fluctuations in generation  $G$  as well and the results are shown in the bottom part of Fig. 10 for a uniformly distributed relative fluctuation of generation  $\delta G/G$  of  $\pm 0.5\%$ . The result is comparable to the effect of temperature fluctuations. In this case, the voltage difference of 0.25 mV and the intensity coefficient of 0.26 mV per % relative generation fluctuation imply a critical limit of 1.0% (thus,  $\pm 0.5\%$ ) where the calculation begins to fail. This marks the minimum requirements to reliably detect an iron contamination of  $1 \times 10^9 \text{ cm}^{-3}$ .

However, having Fig. 1 in mind, the quantification of iron contamination in the low  $1 \times 10^9 \text{ cm}^{-3}$  range is probably not of great importance anyway because its impact on cell performance is limited.

For a contamination of  $1 \times 10^{10} \text{ cm}^{-3}$ , an unrecognized temperature fluctuation of  $\pm 0.05^\circ\text{C}$  renders  $[\text{Fe}]_{\text{app}}$  uncertain to  $\sim 3\%$  (one sigma), whereas an unrecognized generation fluctuation of  $\pm 0.5\%$  renders  $[\text{Fe}]_{\text{app}}$  uncertain to  $\sim 4\%$  (one sigma).

### C. Errors because of Unwanted Association and Dissociation

One possible error source for any method based on the association and dissociation of FeB pairs is the control of the association degree  $Q = [\text{FeB}]/[\text{Fe}]$ , and thus, which portion of iron changes its state and contributes to the measurement. For the two intensity level approach it is even more important because association and dissociation might occur between the measurements at different intensities. More precisely, effective lifetime in the states  $x = (\text{A}1, \text{A}2, \text{B}1, \text{B}2)$  is given by

$$\frac{1}{\tau_{\text{eff},x}} = \frac{1}{\tau_{\text{bg}}} + f_{\text{Fe}} \cdot (1 - Q_x) \cdot [\text{Fe}] + f_{\text{FeB}} \cdot Q_x \cdot [\text{Fe}] \quad (14)$$

and ignoring this in the analysis with the two intensity level approach using (10) will result in a certain error. Therefore, one should be aware of the following.

- 1) The ratio of paired and interstitial iron concentration in thermal equilibrium (i.e., in darkness) follows the empirical relationship [6], [12]:

$$\frac{[\text{FeB}]}{[\text{Fe}_i]} = \frac{N_A}{1 \times 10^{23} \text{ cm}^{-3}} \cdot \exp\left(\frac{0.65 \text{ eV}}{kT}\right) \quad (15)$$

and depends on dopant density  $N_A$ . The association degree at  $25^\circ\text{C}$

$$Q = \frac{[\text{FeB}]}{[\text{Fe}]} = \left(1 + \frac{[\text{Fe}_i]}{[\text{FeB}]}\right)^{-1} \quad (16)$$

is close to unity in the typical range of doping for solar cells, e.g., 99.99% for  $N_A = 1 \times 10^{16} \text{ cm}^{-3}$ , given that a sufficiently long relaxation time is granted.

- 2) Association, i.e., relaxation toward thermal equilibrium, occurs in form of an exponential decay, i.e.  $[\text{Fe}_i](t) = [\text{Fe}] \cdot \exp(-t/t_{\text{as}})$ , with a time constant [7], [12]

$$t_{\text{as}} = \frac{4.3 \times 10^5 \text{ cm}^{-3}}{N_A} \cdot T \cdot \exp\left(\frac{0.68 \text{ eV}}{kT}\right). \quad (17)$$

Hence, association time in the typical range of doping for solar cells is around one hour at room temperature, e.g.,  $t_{\text{as}} = 65 \text{ min}$  for  $N_A = 1 \times 10^{16} \text{ cm}^{-3}$  and  $25^\circ\text{C}$  meaning that interstitial iron is lost with a rate of  $\sim 1.5\%$  per min. Using a sequence of flashes of different intensity in rapid succession is advisable to minimize association related errors, in particular, for the measurement of the *after* state where iron is mainly present as interstitial species  $\text{Fe}_i$ . Almost complete association (99%) may be expected if the sample is left in darkness for  $5 \times t_{\text{as}}$  taking the actual storing temperature into account.

- 3) Almost complete dissociation of FeB pairs can be achieved by intense illumination exceeding  $100 \text{ mWcm}^{-2}$  (white light, 1 sun) for 5 min at room temperature [12]. In contrast, thermal dissociation by annealing at elevated temperature, where the association degree follows (16), may be systematically incomplete even after prolonged annealing because of temperature being chosen too low, e.g.,  $Q = 7\%$  at  $300^\circ\text{C}$ , or a too slow cool-down promoting accelerated association [12].
- 4) Unwanted dissociation of FeB because of illumination during handling and measurement might play a role especially for the sample in the *before* state. Macdonald *et al.* [12] concluded that a deposited power of  $10 \text{ mJcm}^{-2}$  might be acceptable. Following this statement, a 100 ms flash with an intensity of  $100 \text{ mWcm}^{-2}$  (1 sun) for the high intensity measurement would be acceptable. Performing both measurements without sample handling in room light in between and taking the low intensity measurement first might be advisable to minimize dissociation related errors in the two intensity level approach.

In order to estimate the error because of unrecognized association or dissociation in between high ( $\text{A}1, \text{B}1; 62 \text{ mWcm}^{-2}$ ) and low ( $\text{A}2, \text{B}2; 50 \text{ mWcm}^{-2}$ ) intensity measurement in the two intensity level approach, PC1D simulations were repeated assuming different degrees of FeB association  $Q$ , i.e., effective lifetime is given by (16). In particular, it was assumed that association and dissociation was complete during the first measurement, i.e.,  $Q_{\text{B}1} = 1$  and  $Q_{\text{A}1} = 0$ , whereas dissociation and association were varied up to 10% for the second measurement, i.e.,  $1.0 \geq Q_{\text{B}2} \geq 0.9$  and  $0.1 \geq Q_{\text{A}2} \geq 0.0$ . This effect was ignored during subsequent analysis of  $[\text{Fe}]_{\text{app}}$  according to (10). The contour plot in Fig. 11 exemplarily shows the result for

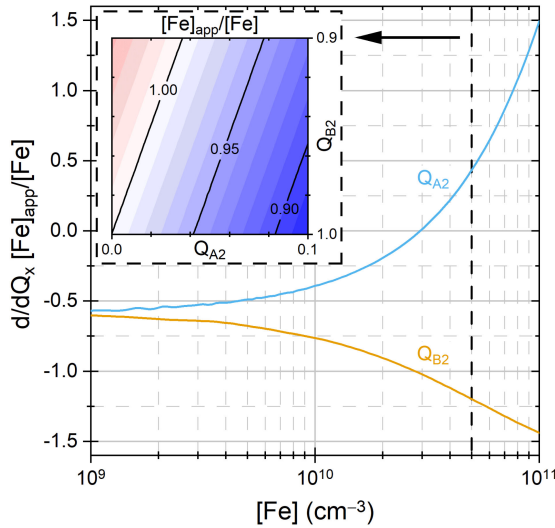


Fig. 11. Contour plot shows the ratio of apparent  $[Fe]_{\text{app}}$  and true  $[Fe]$  iron contamination at  $[Fe] = 5 \times 10^{10} \text{ cm}^{-3}$  in dependence of the FeB association degree  $Q_x$  in the states A2 and B2 being erroneously neglected in the analysis. The line graph shows the derivative of  $[Fe]_{\text{app}}/[Fe]$  with respect to  $Q_{A2}$  and  $Q_{B2}$  in dependence of the true iron contamination  $[Fe]$ .

$[Fe] = 5 \times 10^{10} \text{ cm}^{-3}$ . As can be seen from the straightness and parallelity of the contour lines, the ratio  $R = [Fe]_{\text{app}}/[Fe]$  of apparent and true iron contamination is (at least for small changes) well approximated by

$$R = R|_0 + \frac{dR}{dQ_{A2}}|_0 \cdot \delta Q_{A2} + \frac{dR}{dQ_{B2}}|_0 \cdot \delta Q_{B2} \quad (18)$$

meaning that the deviation corresponds to the linear superposition of the individual changes  $\delta Q_{A2}$  and  $\delta Q_{B2}$  scaled with the first derivative. This is true in the shown iron contamination range up to  $1 \times 10^{11} \text{ cm}^{-3}$  even though the derivative even changes its sign. For  $[Fe]$  above  $1 \times 10^{11} \text{ cm}^{-3}$ , the analysis increasingly underestimates the true iron contamination resulting in stronger nonlinear behavior not discussed here. It is interesting to note that  $[Fe]_{\text{app}}$  always underestimates  $[Fe]$  below  $3 \times 10^{10} \text{ cm}^{-3}$ , whereas it is possible to overestimate  $[Fe]_{\text{app}}$  above that contamination level.

Having the association and dissociation behavior discussed before in mind, it should be possible to limit dissociation in between B1 and B2 (*before*) measurements if both measurements are performed in rapid succession with a flasher system using short flashes. FeB pairs dissociated before the first measurement are not covered by the measurement in general. Furthermore, it should be possible to limit unwanted association in between A1 and A2 (*after*) measurements to below 1% if the measurements are performed within a few seconds.

#### D. Other Error Sources

Lateral variation in material quality ( $j_0$ ) gives rise to lateral compensation currents not covered by the shown PC1D simulations, and thus, the measured  $V_{\text{oc}}$  is a result of lateral averaging. It is hard to predict in a general way what the impact of lateral inhomogeneity is, especially if iron is inhomogeneously distributed as well.

Furthermore, it should be noted that iron is not the only recombination active defect species changing its state by illumination and/or annealing at elevated temperature. For example, chromium is known to switch between interstitial ( $\text{Cr}_i$ ) and paired state ( $\text{CrB}$ ) as well. In addition, boron-oxygen related defects are known to degrade lifetime at room temperature under illumination as well [24]). It is therefore recommended to either quantify iron after complete degradation, or to prepare the *after* state first and the *before* state second by storing the sample in darkness at room temperature because the latter treatment does not affect boron-oxygen related defects. Furthermore, light and elevated temperature induced degradation (LeTID) [25] may occur in solar cells as well, however, it is believed to occur not or at least only on long time scales at room temperature, thus, optical dissociation of FeB pairs is to be preferred to thermal dissociation. It cannot be excluded as well that surface passivation changes, especially during thermal dissociation steps.

In any of those cases, the reversibility of FeB pair formation offers the possibility to repeat the (optical) dissociation-association cycle and it might be advisable to check whether apparent iron contamination changes from cycle to cycle.

## V. CONCLUSION

The specific impact of interstitial iron and iron-boron pairs on the electrical parameters of solar cells, in particular on open circuit voltage  $V_{\text{oc}}$ , and the possibility to deliberately switch between those states allows for a quantification of the iron contamination level.

A comparison of  $V_{\text{oc}}$  before and after FeB dissociation with the presented one intensity level approach underestimates iron contamination levels across a large range of contamination from  $10^9$  to  $10^{12} \text{ cm}^{-3}$  to some extent depending on the base doping. This underestimation is a direct consequence of the mismatch of injection present at  $V_{\text{oc}}$  before and after FeB dissociation (implying that the non-iron related background lifetime is probed at different injection levels), and the neglected injection dependence of this non-iron related background lifetime. A variation of illumination intensity might be useful in order to shift the analysis to an injection region where background lifetime changes less.

Adding information by measuring at two intensity levels before and after FeB dissociation allows for a better assessment of background lifetime injection dependence and allows for an even more accurate quantification of the iron contamination level.

Systematic measurement errors or erroneous assumptions on temperature, generation and doping level are probable error sources that yield systematic errors in the single digit percentage range. However, the more relevant error source for application are probably unrecognized fluctuations in temperature and generation between the measurements before and after FeB dissociation defining what contamination level can be reliably resolved.

In principle, the presented approach should work with the dissociation of FeGa pairs as well as these show a comparable switching behavior and injection dependence [8], [26]. However, the exact recombination parameters of FeGa pairs are still subject to discussion [8].

## APPENDIX

The one diode model, here written in  $V_{oc}$  conditions

$$0 = j(V_{oc}) = j_0 \cdot \left[ \exp\left(\frac{qV_{oc}}{kT}\right) - 1 \right] - j_{ph} \quad (19)$$

links  $V_{oc}$  to photo-generated current density  $j_{ph}$ . The exponential function is by far larger than unity at  $V_{oc}$  and, thus, the subtraction of unity can be neglected in the following.  $j_{ph}$  can be assumed to scale linearly with generation rate  $G$  or better normalized generation rate  $g = G/G_0$ , thus,  $j_{ph} = x \cdot g$  with  $x$  corresponding to the photo-generated current  $j_{ph}$  at reference generation  $G_0$ . Solving for  $V_{oc}$  yields

$$V_{oc} = \frac{kT}{q} \cdot \ln\left(\frac{x \cdot g}{j_0}\right). \quad (20)$$

Partial derivation with respect to generation then yields

$$\frac{\partial V_{oc}}{\partial g} \Big|_{g=1} = \frac{kT}{q} \cdot \frac{j_0}{x \cdot g} \cdot \frac{x}{j_0} = \frac{kT}{q} \cdot \frac{1}{g} = \frac{kT}{q} \quad (21)$$

with  $kT/q \sim 25.7$  mV at 25 °C.

Partial derivation with respect to temperature yields

$$\frac{\partial V_{oc}}{\partial T} = \underbrace{\frac{k}{q} \cdot \ln\left(\frac{x \cdot g}{j_0}\right)}_{V_{oc}/T} - \frac{kT}{q} \cdot \frac{1}{j_0} \cdot \frac{\partial j_0}{\partial T} \quad (22)$$

depending on the derivative of the saturation current density  $j_0$ .

For an infinite diode and constant lifetime, it is given by

$$j_0 = c \cdot n_i^2 = c \cdot T^3 \exp\left(-\frac{E_g}{kT}\right) \quad (23)$$

hence

$$\begin{aligned} \frac{\partial j_0}{\partial T} &= \underbrace{3 \cdot cT^2 \exp\left(-\frac{E_g}{kT}\right)}_{j_0/T} - \underbrace{cT^3 \exp\left(-\frac{E_g}{kT}\right)}_{j_0} \cdot \frac{\partial}{\partial T} \frac{E_g}{kT} \\ &= j_0 \cdot \left( \frac{3}{T} - \frac{1}{kT} \frac{\partial E_g}{\partial T} + \frac{E_g}{kT^2} \right) \end{aligned} \quad (24)$$

where the band gap  $E_g$  decreases approximately linearly with temperature at a rate of  $-0.25$  meV per °C. In summary

$$\frac{\partial V_{oc}}{\partial T} = \underbrace{\frac{1}{T} \left( V_{oc} - \frac{E_g}{q} \right)}_{-1.5mV/K} + \underbrace{\left( \frac{1}{q} \frac{\partial E_g}{\partial T} - \frac{3k}{q} \right)}_{-0.5mV/K}. \quad (25)$$

However, a real solar cell of finite thickness does not behave like an ideal infinite diode with constant lifetime and the change in  $V_{oc}$  with temperature of a good solar cell is typically rather in the range of  $-1.5$  mV per °C. Nevertheless it depends on  $V_{oc}$  level.

## REFERENCES

- [1] A. Haarahlitunen, H. Savin, M. Yli-Koski, H. Talvitie, and J. Sinkkonen, "Modeling phosphorus diffusion gettering of iron in single crystal silicon," *J. Appl. Phys.*, vol. 105, no. 2, Jan. 2009, Art. no. 023510.
- [2] S. P. Phang and D. Macdonald, "Direct comparison of boron, phosphorus, and aluminum gettering of iron in crystalline silicon," *J. Appl. Phys.*, vol. 109, no. 7, Apr. 2011, Art. no. 073521.
- [3] P. Altermatt *et al.*, "From upscaling PERC to the next technology cycle: Transparent passivating contacts may merge n- and p-type cell technology," in *Proc. 38th Eur. Photovolt. Sol. Energy Conf. Exhib.*, 2021, pp. 100–106.
- [4] J. Schmidt, "Effect of dissociation of iron-boron pairs in crystalline silicon on solar cell properties," *Prog. Photovolt.: Res. Appl.*, vol. 13, no. 4, pp. 325–331, May 2005.
- [5] S. Dubois *et al.*, "Influence of iron contamination on the performances of single-crystalline silicon solar cells: Computed and experimental results," *J. Appl. Phys.*, vol. 100, no. 2, Jul. 2006, Art. no. 024510.
- [6] L. Kimerling and J. Benton, "Electronically controlled reactions of interstitial iron in silicon," *Physica*, vol. 116, no. 1–3, pp. 297–300, Feb. 1983.
- [7] G. Zoth and W. Bergholz, "A fast, preparation-free method to detect iron in silicon," *J. Appl. Phys.*, vol. 67, no. 11, pp. 6764–6771, Jun. 1990.
- [8] T. U. Nærland *et al.*, "On the recombination centers of iron-gallium pairs in ga-doped silicon," *J. Appl. Phys.*, vol. 122, no. 8, Aug. 2017, Art. no. 085703.
- [9] A. Richter, S. W. Glunz, F. Werner, J. Schmidt, and A. Cuevas, "Improved quantitative description of auger recombination in crystalline silicon," *Phys. Rev. B*, vol. 86, no. 16, Oct. 2012, Art. no. 165202.
- [10] *Photovoltaic Devices - Part 1: Measurement of Photovoltaic Current-Voltage Characteristics*, IEC Standard 60904–1, 1987.
- [11] A. Herguth, "On the meaning(fullness) of the intensity unit 'suns' in light induced degradation experiments," *Energy Procedia*, vol. 124, pp. 53–59, Sep. 2017.
- [12] D. H. Macdonald, L. J. Geerligs, and A. Azzizi, "Iron detection in crystalline silicon by carrier lifetime measurements for arbitrary injection and doping," *J. Appl. Phys.*, vol. 95, no. 3, pp. 1021–1028, Feb. 2004.
- [13] D. Macdonald, T. Roth, P. N. K. Deenapanray, T. Trupke, and R. A. Bards, "Doping dependence of the carrier lifetime crossover point upon dissociation of iron-boron pairs in crystalline silicon," *Appl. Phys. Lett.*, vol. 89, no. 14, Oct. 2006, Art. no. 142107.
- [14] W. Shockley and W. T. Read, "Statistics of the recombinations of holes and electrons," *Phys. Rev.*, vol. 87, no. 5, pp. 835–842, Sep. 1952.
- [15] R. N. Hall, "Electron-hole recombination in germanium," *Phys. Rev.*, vol. 87, no. 2, pp. 387–387, Jul. 1952.
- [16] A. Istratov, H. Hieslmair, and E. Weber, "Iron contamination in silicon technology," *Appl. Phys. A: Mater. Sci. Process.*, vol. 70, no. 5, pp. 489–534, May 2000.
- [17] A. Herguth, "On the application of lifetime-equivalent defect densities on solar cell level," *IEEE J. Photovolt.*, vol. 11, no. 6, pp. 1410–1418, Nov. 2021.
- [18] R. A. Sinton and A. Cuevas, "Contactless determination of current-voltage characteristics and minority-carrier lifetimes in semiconductors from quasi-steady-state photoconductance data," *Appl. Phys. Lett.*, vol. 69, no. 17, pp. 2510–2512, Oct. 1996.
- [19] M. J. Kerr, A. Cuevas, and R. A. Sinton, "Generalized analysis of quasi-steady-state and transient decay open circuit voltage measurements," *J. Appl. Phys.*, vol. 91, no. 1, pp. 399–404, Jan. 2002.
- [20] D. Kane and R. Swanson, "Measurement of the emitter saturation current by a contactless photoconductivity decay method (silicon solar cells)," in *Proc. 18th IEEE Photovolt. Specialists*, Las Vegas, NV, USA, 1985, pp. 578–583.
- [21] K. R. McIntosh and L. E. Black, "On effective surface recombination parameters," *J. Appl. Phys.*, vol. 116, no. 1, Jul. 2014, Art. no. 014503.
- [22] PV Lighthouse, "Band gap calculator," Accessed: Oct. 4, 2021. [Online]. Available: <https://www.pvlighthouse.com.au/bandgap>
- [23] H. Haug and J. Greulich, "PC1Dmod 6.2 – Improved simulation of C-Si devices with updates on device physics and user interface," *Energy Procedia*, vol. 92, pp. 60–68, Aug. 2016.
- [24] T. Niewelt, J. Schon, W. Warta, S. W. Glunz, and M. C. Schubert, "Degradation of crystalline silicon due to boronoxygen defects," *IEEE J. Photovolt.*, vol. 7, no. 1, pp. 383–398, Jan. 2017.
- [25] J. Schmidt, D. Bredemeier, and D. C. Walter, "On the defect physics behind light and elevated temperature-induced degradation (LeTID) of multicrystalline silicon solar cells," *IEEE J. Photovolt.*, vol. 9, no. 6, pp. 1497–1503, Nov. 2019.
- [26] R. Post, T. Niewelt, J. Schön, F. Schindler, and M. C. Schubert, "Imaging interstitial iron concentrations in gallium-doped silicon wafers," *Phys. Status Solidi (A)*, vol. 216, no. 10, Jan. 2019, Art. no. 1800655.